

THE EFFECT OF SLOW HEATING RATES ON THE REACTION MECHANISMS OF NANO AND MICRON COMPOSITE THERMITE REACTIONS

Michelle L. Pantoya* and J. J. Granier

Department of Mechanical Engineering, Texas Tech University, Lubbock, Texas 79409, USA

Thermal analyses were performed on Al+MoO₃ thermite reactions as a function of Al particle size (ranging from 50 to 20 µm) and heating rate (from 2.5 to 15 K min⁻¹). Results include ignition (onset) temperatures and heats of reaction. The nano-thermitites initiate prior to reactant phase changes and at least 300°C below micron-thermitites. The differences in ignition temperatures are suggestive of different ignition mechanisms. Nano-thermitites display higher heats of reaction that are dependent on experimental conditions.

Keywords: heat of reaction, ignition temperature, nano-aluminum, nanocomposite, thermites

Introduction

Recent studies on nanocomposite thermites, particularly metastable interstitial composites (MICs), suggest that the reaction mechanism is not only a function of the particle size but also greatly dependant on the heating rate. MICs or nanocomposite thermites use nano-scale aluminum (Al) particles as the fuel component combined with nano-scale metal oxidizer particles to generate highly exothermic reactions. The reduction of particle size from micron-scale to nano-scale has increased the reactivity of the Al particles such that the composite exhibits greater ignition sensitivity and increased reactive power [1–4].

The role of particle size is evident when examining the thermal behavior of the MIC. Most notable is that the nanocomposites react well before Al melting, while micron-composites react at temperatures exceeding the Al melting point [4]. Previous work also showed that the onset and peak temperatures for Al/MoO₃ reactions are affected by the Al size distributions with those for narrow-size distribution samples being approximately 50°C higher than those for broad-size distribution samples [4].

Experiments have also indicated that variations in the heating rate affect the ignition and reaction mechanism of the composite. For example, Dlott *et al.* showed that nano-Al particles coated with relatively thicker passivation shells promote increased pressure buildup for shock ignition scenarios [5]. Although thicker shells may be advantageous for high heating rate initiation, they are a detriment for slow heating rate initiation. The passivation shell is composed of alumina (Al₂O₃), which acts as a heat sink and will im-

pede energy transport when heated at slower rates. Other work by Zachariah *et al.* showed that ignition temperatures of nano-Al particles exceed the melting point when heated at heating rates exceeding 1000 K min⁻¹ [6]. These variations in ignition behaviors, such as onset or ignition temperature are clearly a function of the heating rate. In an effort to understand the influence of slow heating rates on ignition (onset) temperature, differential scanning calorimeter (DSC) experiments were performed that examine the heat flow as a function of heating rate ranging from 2.5 to 15 K min⁻¹ and as a function of Al particle size ranging from 50 nm to 20 microns.

Experimental

Sample preparation

Thermites were prepared from spherical Al and nano-crystalline MoO₃ particles. Approximately one gram of thermite powder was prepared for eight Al particle sizes listed in Table 1. In Table 1, the ‘product size’ refers to the average particle diameter and ‘purity’ refers to the actual Al content. The ‘calculated oxide thickness’ was derived based on the average particle diameter and Al purity.

All of the thermite reactants were mixed at a slightly fuel rich stoichiometry, and sonicated in a hexane solution to break up agglomerates and improve the homogeneity of the mixture. The hexane evaporated for 15 min on a 60°C hotplate and the homogeneous powder mixture was then ready for testing. For further information of thermite mixing and preparation the reader is referred to [2].

* Author for correspondence: michelle.pantoya@coe.ttu.edu

Table 1 Physical property data for thermite reactants

Material	Product size	Manufacturer	Purity/%	Calculated oxide thickness/nm
aluminum	50 nm	nanotechnologies	75.0	1.69
	80 nm	nanotechnologies	84.0	1.63
	120 nm	nanotechnologies	81–82	2.87
	1–3 µm	Atlantic Equipment Engineers (AEE)	99.9	0.23
	3–4 µm	Alfa Aesar	98.5	6.17
	4.5–7 µm	Alfa Aesar	98.5	10.13
	10–14 µm	Alfa Aesar	98.5	21.14
	20 µm	Sigma Aldrich	99.9	2.33
molybdenum trioxide		climax	99.9	

Methods

Thermal analysis measurements were made using a simultaneous TG/DSC (thermogravimetric/differential scanning calorimetry) apparatus (Netzsch model STA 409PC/4/H/CO Luxx). Measurements were made in a flowing argon atmosphere and the furnace provided a measuring temperature range between ambient (22°C) and 1450°C.

The DSC system was first evacuated with a diaphragm pump (KNF model N 813.3 ANE) and then evacuated to $<2 \cdot 10^{-4}$ mbar with a turbomolecular drag pump (Pfeiffer model TMU 071 P). The system was back-filled with standard grade argon gas (99.9993% purity) until reaching atmospheric pressure and a valve was opened to allow a constant flow of purge gas through the sample chamber.

A platinum sample carrier and platinum crucibles allowed temperature measurements in the higher temperature range without radiation effects. An alumina liner was inserted into the platinum crucibles since platinum is reactive with many metals (like aluminum) at elevated temperatures. A thin platinum lid with a small hole (to prevent gas pressure build up) was used to improve heat containment. The platinum-alumina crucibles measure 6 mm internal diameter and 2.3 mm deep. This crucible volume allowed for approximately 16 mg of loose powder sample. The sample mass for all of the Al powder (nano and micron) was kept between 4 and 6 mg in order to minimize the violence of any reactions inside the furnace. Each sample mass was input into the computer prior to the experiment to allow a mass normalization of enthalpy calculations (this mass is also adjusted and tared by the TG for enthalpies during mass loss or gain).

After each sample was tested, the crucible was removed from the sample carrier and cleaned. The solid products were retrieved from the alumina liner with a needle or metal probe and stored for SEM analysis. The platinum-alumina crucible was then placed in a 10% NaOH solution to generate bubble agitation by reacting with any remaining aluminum.

After settling, the platinum-alumina crucible was rinsed with distilled water and placed in a sonic bath of distilled water for 3–5 min. The platinum-alumina crucible was loosely dried and placed on 200°C hotplate such that the remaining water was removed. The heating process would usually cause the alumina liner to unseat itself. The liner and platinum crucible were inspected for flaws and then reseated. The alumina liners are very thin and fragile and would only survive approximately 8 to 10 sonication periods before cracking and being replaced.

Results

Figure 1 presents TG/DSC data from the Al and MoO₃ reactants tested separately. The left solid line valley displays the endothermic melt of a 17 mg sample of 120 nm-Al. The right solid line valley displays the endothermic sublimation of a 12.2 mg sample of the nano-scale MoO₃ with a subsequent mass loss from the sublimed gas leaving the crucible (TG mass loss is illustrated by the dashed line). Figure 1 shows how the onset temperatures are calculated based on intersection of tangential lines. As expected the 120 nm-Al shows an onset temperature of 644.8°C (compared to ASTM value

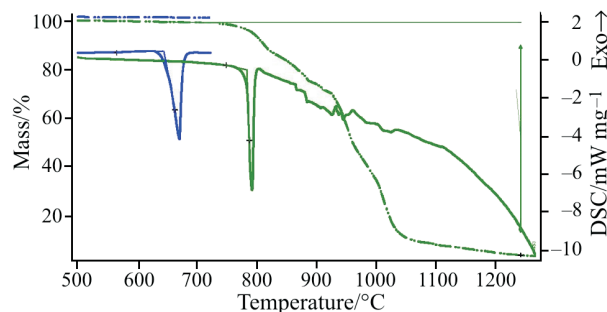


Fig. 1 TG/DSC curves of 120 nm Al melt and MoO₃ sublimation (both at 10 K min⁻¹ in an argon environment). Al melt endotherm has an onset temperature of 644.9°C. MoO₃ sublimation onset occurs at 783.6°C. The dashed line indicates TG mass loss for MoO₃ during sublimation is 95.85%

of 660.3°C [7]), peaks at 671°C and then returns to the baseline with no mass change. The MoO_3 begins to sublime at 700°C and melts at 795°C [8]. In Fig. 1 MoO_3 shows an onset temperature of 783.6°C . The [8] data is consistent with Fig. 1 because the DSC curve begins to fall beneath a flat baseline at 700°C as the sample is gradually sublimed and the mass is reduced, dropping the sample heat capacity and heat flow signal.

Figure 2 is TG/DSC analyses from $40\text{ nm-Al} + \text{MoO}_3$ showing an exothermic reaction starting at 265.5°C (onset), peaking at 507.2°C with an enthalpy (area under the curve) of 2441 J g^{-1} . Before the exothermic reaction reaches completion, the remaining Al in the sample melts showing an overlapping endothermic melt peaking at 658.1°C .

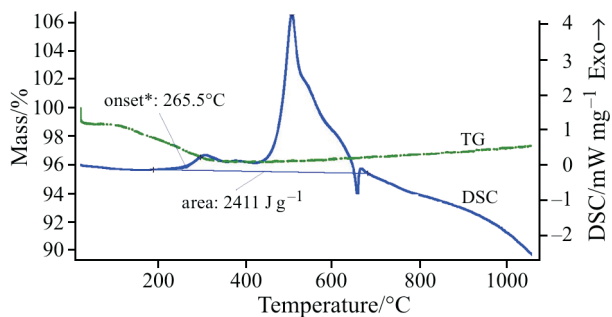


Fig. 2 TG/DSC curves of $40\text{ nm-Al} + \text{MoO}_3$ reaction. This 12.1 mg sample was heated at 10 K min^{-1} in argon. Onset temperature is 265.5°C and peak temperature is 507.2°C . Area under the exotherm corresponds to 2441 J g^{-1} . The peak for the Al melting endotherm occurs at 658.1°C

Figure 3 is TG/DSC analyses from $3\text{--}4.5\text{ }\mu\text{m-Al} + \text{MoO}_3$ showing an exothermic reaction starting at 522.2°C (onset), peaking at 889.6°C with an enthalpy (area under the curve) of 4012 J g^{-1} . In this same temperature range (i.e. between the onset and end temperatures of the exothermic peak) the Al content of the sample shows endothermic melt and the MoO_3 content in

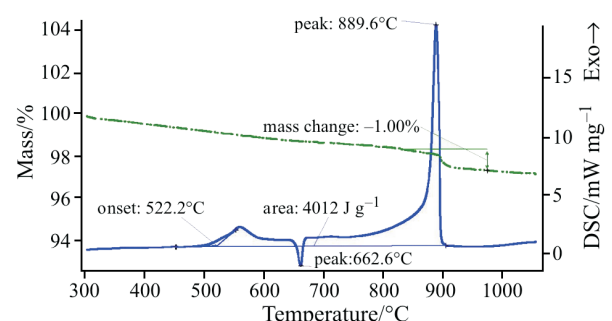


Fig. 3 TG/DSC curves of $3\text{--}4.5\text{ }\mu\text{m-Al} + \text{MoO}_3$ reactions (10 K min^{-1} in argon). The 17.1 mg sample shows an onset temperature of 522.2°C and a peak temperature of 889.6°C with a 1% mass change (dashed line corresponds with TG mass loss data)

the sample transitions by sublimation indicated by the TG mass loss (dashed line) starting around 800°C .

Similar experiments were conducted for all of the Al particle sizes shown in at heating rates ranging from 2.5 to 15 K min^{-1} . Similar to Figs 2 and 3, all of the nano-thermites begin reacting prior to the Al melt and in the solid-state. Whereas the main exothermic reaction for all micron-thermites may begin in the solid-state but peaks well above phase transition temperatures of Al ($T_{\text{mp}}=660^{\circ}\text{C}$ [7]) and MoO_3 ($T_{\text{sublime}}=790^{\circ}\text{C}$ [7]).

Figure 4 shows the onset temperature as a function of Al particle size for the main exothermic reactions of each thermite. The figure shows four data points for each Al particle size differing by the DSC heating rate and the average onset temperature for each Al particle size. The onset temperatures for the micron thermites were determined based on the main exothermic reaction (similar to the larger peak in Fig. 3).

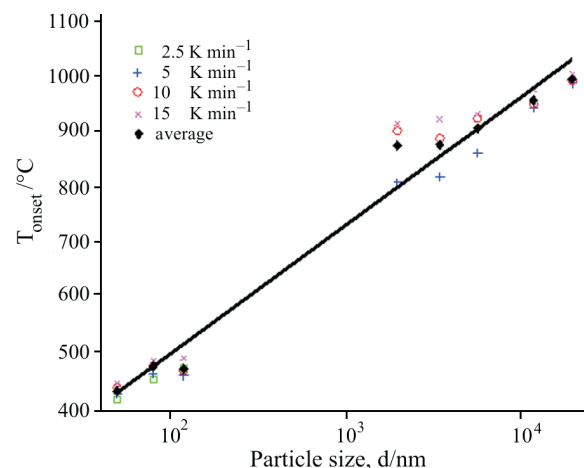


Fig. 4 Onset temperature for $\text{Al} + \text{MoO}_3$ reactions in argon as a function of Al particle size for various heating rates

Figure 5 shows the heats of reaction (ΔH) determined by an area calculation under the heat flow curve (e.g. Figs 2 and 3). Prior to each experiment the DSC was calibrated for a specific crucible and heating rate using a 21.2 mg sapphire sample with a known specific heat. This calibration allowed the temperature and voltage signals to be converted to enthalpy measurements. The first trend present in Fig. 5 is the logarithmic decrease in ΔH with increase Al particle size. The second trend is the variation of heats of reaction as a function of heating rate for each individual Al particle size. The nano-thermites show the highest ΔH for the slowest heating rate (2.5 K min^{-1}) with decreasing ΔH with increasing heating rate. The enthalpy values are defined by a start and end point corresponding to estimated divergence from and returning to a flat baseline curve. Most of the nano-thermites do not complete the

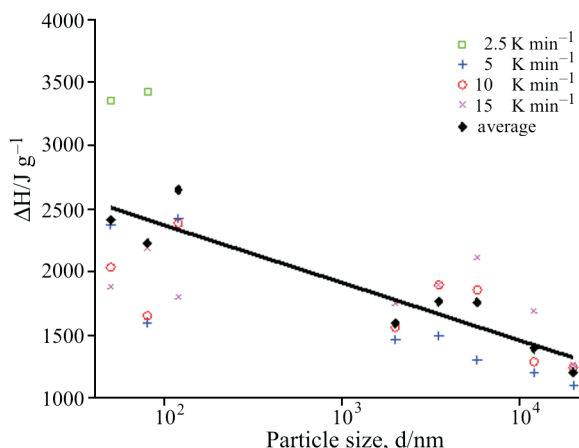


Fig. 5 DSC heat of reaction for Al+MoO₃ reactions in argon as a function of Al particle size for various heating rates

exothermic reaction before reaching the melting temperature of Al (e.g. Fig. 2 and shown more definitively in the 5 and 2.5 K min⁻¹ nano-thermite heat flow curves). For this reason, the heats of reaction are inaccurate due to the competing positive and negative energy signals. An optimized curve would show all reactions distinctly with each peak (or valley) returning to the baseline prior to a subsequent peak (or valley). The typical method of resolving the peaks is to slow the heating rate. The three nano-thermites were then tested at 2.5 K min⁻¹ with no success of resolving independent peaks. This result led to further testing to characterize the temperature dependent reactions.

The controlled heating of the DSC allowed the Al+MoO₃ samples to react relatively slow such that most reactions left a solid product in the crucible after reacting. At higher heating rates as achieved through laser or spark ignition [1–3], the highly exothermic reaction disperses products. For this reason, capturing products is difficult and thus products of the reaction have not been thoroughly studied.

Visual observation of the reactants and products were made by comparing scanning electron microscopy (SEM) images. Figures 6a and b show SEM images of 20 µm-Al+MoO₃ reactants and products reacted during a 15 K min⁻¹ DSC heating. The images in the left column show single 20 µm (approximate) Al particles coated in nm-MoO₃ crystals (with a few anomaly large MoO₃ sheets). The images in the right column show a more continuous structure (absent of the large void between micron size particles) with a few distinct crystalline structures. It is speculated that the crystalline structures in the product images are condensed molybdenum (larger crystals and more defined in images b1 and 2).

Figures 7a and b show microscopic images of the reactants and products of 10–14 µm-Al+MoO₃ reacted

in the DSC at 15 K min⁻¹ heating rate. Figure 7a1 shows several micron scale (10–14 µm) Al particles coated in the nm-MoO₃ crystals. Figure 7a2 shows at least two-micron size Al particles coated in MoO₃ with spherical shape and diameters of approximately 18 and 7.5 µm. Unlike the 20 µm-Al+MoO₃ products, Fig. 7b1 does not appear to be as homogeneous and continuous. The product in Fig. 7b1 still show the spherical shape of the micron Al particles that were apparently agglomerated or sintered during the reaction. The 10–14 µm products also show fibrous whiskers (Fig. 7b2). Whisker formation during Al oxidation has been attributed to the rapid deposition (or solidification) of vaporized Al₂O₃ products [7, 9, 10].

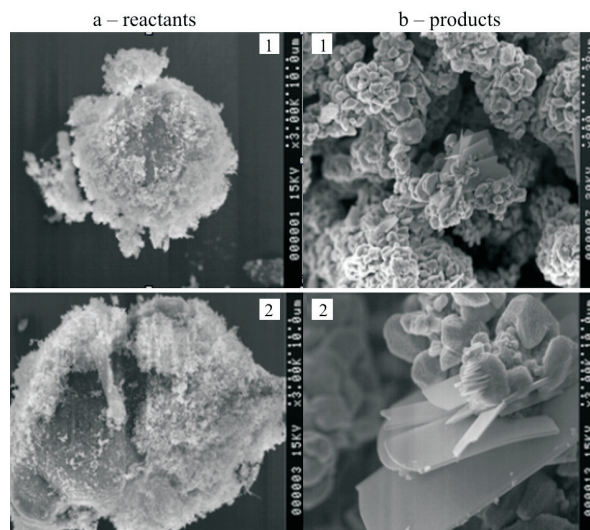


Fig. 6 SEM images of 20 µm-Al+MoO₃ a – before and b – after combustion

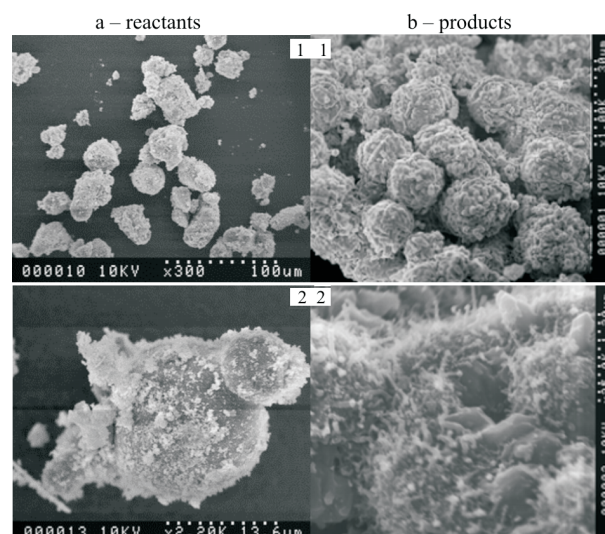


Fig. 7 SEM images of 10–14 µm-Al+MoO₃ a – before and b – after combustion

Discussion

Nano-thermites ignite at lower temperatures than micron-thermites. The three nano-thermites show an average T_{onset} of 455.7°C, which is lower than the Al melting temperature or MoO₃ sublimation suggesting a solid–solid reaction. Based on the largest exothermic peak in DSC experimental data, the micron-thermites show an average T_{onset} between 874.6 and 994.5°C for 1–3 and 20 μm, respectively and above the phase transition temperatures of both reactants, indicating a liquid Al and gaseous MoO₃ reactant state.

A theory explaining the differences in onset temperature is presented based on surface area variations of Al particles. Aluminum particles are composed of a pure Al core surrounded by an alumina shell. An approximation can be made for the average dimension of the Al core and oxide thickness for a single particle for each of the Al samples tested. Using the Al purity data from Table 1 a set of simultaneous equations using dimensional congruency and mass conservation can be derived. The densities for the possible constituents of a single Al particle are shown in Table 2.

Table 2 Al particle constituent densities (kg m⁻³)

Al	amorphous Al ₂ O ₃	γ-phase Al ₂ O ₃
2698.4	3050	3660

All calculations are made for a single average particle diameter, d (i.e. the micron particles are given in a range such as 10–14 μm, which will be represented by 12 μm for calculations). The first equation can be derived simply by particle geometry where x is the true Al core radius and y is the oxide shell thickness.

$$x+y=d/2 \quad (1)$$

The second equation is the combination of the following two-mass balance equations where m is the total mass of a single particle and P is the Al purity (Table 1).

$$4/3\pi x^3 \rho_{\text{Al}} = Pm \quad (2)$$

$$4/3\pi[(y+x)^3 - x^3] \rho_{\text{Al}_2\text{O}_3} = (1-P)m \quad (3)$$

Solving for m and equating Eqs (2) and (3) yields Eq. (4).

$$\begin{aligned} 4/3\pi x^3 \rho_{\text{Al}} &= \\ &= \left(\frac{P}{1-P} \right) (4/3\pi[(y+x)^3 - x^3] \rho_{\text{Al}_2\text{O}_3}) \end{aligned} \quad (4)$$

Assuming that the Al samples are delivered with an amorphous oxide layer (using the amorphous oxide density) the core radius and oxide thicknesses were calculated as shown in Table 2.

Dreizen states that at about 550°C, the amorphous oxide layer exceeds its critical thickness and amorphous alumina transforms into γ-phase Al₂O₃ [11]. This transformation causes drastic changes in the mechanical properties of the oxide layer. Because of the 20% density increase (shown in Table 2), the γ-Al₂O₃ actually shrinks and exposes regions of the Al core allowing faster diffusion pathways. Based on Dreizen's work another series of equations are derived to compare the surface area changes during the amorphous to γ-Al₂O₃ transformation.

Assuming the particle is instantaneously unreacting at the moment of phase-transformation, the mass of Al₂O₃ will remain constant, and is calculated by Eq. (5).

$$\begin{aligned} m_{\text{Al}_2\text{O}_3} &= \rho_{\text{amorph-Al}_2\text{O}_3} vol_{\text{amorph-Al}_2\text{O}_3} = \\ &= \rho_{\text{amorph-Al}_2\text{O}_3} [4/3\pi(d/2)^3 - x^3] = \\ &= \rho_{\text{amorph-Al}_2\text{O}_3} [4/3\pi(r_{\text{ext}}^3 - r_{\text{int}}^3)] \end{aligned} \quad (5)$$

The new volume for the γ-Al₂O₃ can then be calculated using the appropriate density.

$$vol_{\gamma-\text{Al}_2\text{O}_3} = \frac{m_{\text{Al}_2\text{O}_3}}{\rho_{\gamma-\text{Al}_2\text{O}_3}} \quad (6)$$

Assuming that the oxide layer stays a consistent thickness and only shrinks radially around the Al core, the following simultaneous equations can be solved for an effective γ-Al₂O₃ interior and exterior radius.

$$vol_{\gamma-\text{Al}_2\text{O}_3} = 4/3\pi(r_{\text{ext}}^3 - r_{\text{int}}^3) \quad (7)$$

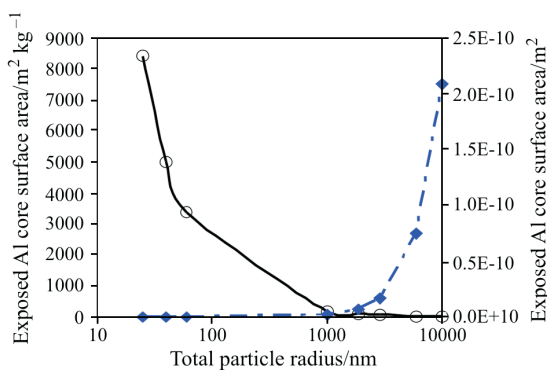
$$r_{\text{ext}} - r_{\text{int}} = y \quad (8)$$

Assuming that the Al core radius does not change, the available surface area coverage by the γ-Al₂O₃ layer can be calculated using the interior radius from above. The values of each of the effective interior radii are shown in Table 3.

Figure 8 shows the surface area change for a single Al particle on the right y -axis as a function of the original particle radius (from the manufacturer). Obviously, the 20 μm particles (10000 nm radius) have a large volume of Al oxide and much higher surface area than smaller nano particles resulting in a significantly larger Al core exposure for a single particle. The key to comparing the reactions of nano and micron Al particles is analyzing the surface area characteristics on a per Al mass basis. The mass of Al in a single micron particle can be represented by millions of nano-particles to achieve the same mass. Thus, Fig. 8 also shows data normalized on an Al mass basis (left curve, left y -axis). In summary, for a single kg of nano-Al, the oxide phase transformation may expose 8000 times the surface area of pure Al (cores) than a kg of micron-Al.

Table 3 Particle geometry calculations

Original particle radius/nm	Particle purity/%	Al core radius (interior α -phase oxide radius)/nm	Oxide thickness/nm	Effective interior γ -phase oxide radius/nm
25	75.0	22.94	2.06	20.85
40	84.0	37.98	2.02	34.58
60	81.5	56.45	3.55	51.38
1000	99.0	997.04	2.96	910.04
1875	98.5	1866.70	8.35	1703.70
2875	98.5	2862.20	12.80	2612.30
6000	98.5	5973.30	26.71	5451.70
10000	99.0	9970.40	29.61	9100.40

**Fig. 8** Surface area change during oxide phase transformation for a single particle and per Al mass

Experiments confirm incomplete reactions that are a function of heating rates and Al particle size. Theoretically ΔH will remain constant and is dependent only on thermodynamic and chemical properties for the Al+MoO₃ global reaction [12]. Figure 5 shows that the nano-thermite heats of reaction dramatically decrease with increasing heating rate. Images support the existence of unreacted particles in product residue. In a comparison of heating rate effects, the three nano-thermite reactions are path dependent, displaying variable ΔH_{rxn} depending on the heating rate. The nano-thermites heated at 2.5 K min⁻¹ display an average (of the three nano-particle sizes) ΔH_{rxn} of 3596 J g⁻¹, which is reduced to an average ΔH_{rxn} of 1962 J g⁻¹ for the 15 K min⁻¹ experiments. This suggests that the reaction is proceeding differently based on heating rate and that the process is preventing complete reaction of all of the reactants (preventing the maximum energy production).

In a comparison of ΔH vs. Al particle size, Fig. 5 shows that the micron-thermites consistently produce lower heats of reaction than the nano-thermites. Models of Al oxidation [13–15] combined with experimental results in this work suggest that the opposing processes of Al₂O₃ growth vs. the formation of Al₂O₃ diffusion barriers prevents the micron-thermites from completely reacting. In summary, as the micron reaction proceeds, each Al particle forms thicker organized

Al₂O₃ layers. This oxide layer eventually prevents any diffusion before the total Al core mass is consumed. Thus the micron-thermites ΔH values shown Fig. 5 are representative of even more incomplete reactions than the nano-thermites.

The Al+MoO₃ reaction is diffusion limited and heavily effected by the temperature and heating rate. This is shown in the variability in ΔH for a single Al particle size for different heating rates. For example, the 40 nm Al+MoO₃ thermite in Fig. 2 is shown at 10 K min⁻¹. For a 10 K min⁻¹ temperature program, the reaction begins at approximately 265°C (27.1 min) and completes at approximately 693°C (68.5 min) resulting in a reaction duration of 41.4 min that is used in determining the time integral ΔH_{rxn} value. Now considering the slower heating rate, and because the reaction progress is dependent of temperature it can be shown that a 40 nm Al+MoO₃ sample reacts in approximately the same temperature interval ($\Delta T=428^\circ\text{C}$). Doing a simple calculation based on the temperature change for a 2.5 K min⁻¹ heating rate, the reaction duration would be approximately 171.2 min. This significant increase in reaction duration is one explanation for the elevated ΔH values for the nano-thermites at slow heating rates. Conversely, the micron-thermite reactions are not as temperature dependent (e.g. right hand side of Fig. 5) resulting in a smaller variability with altering heating rates. Another explanation for the heating rate influences on ΔH is simply that the slower heating rates allow for more sensitive measurements. The slow heating rates may allow the reaction energy to be transferred to the DSC thermocouples more efficiently allowing for a more accurate measurement of the actual heat release.

Acknowledgements

The authors gratefully acknowledge support from the Army Research Office under grant number W911NF-04-1-0217. We are also thankful for support provided by the National Science Foundation under grant number CST-021014 and our program manager, Dr. Linda Blevins.

References

- 1 M. L. Pantoya and J. J. Granier, Prop., Expl., Pyro., 30 (2005) 1.
- 2 J. J. Granier and M. L. Pantoya, Comb. Flame, 138 (2004) 373.
- 3 B. S. Bockmon, M. L. Pantoya, S. F. Son, B. W. Asay and J. T. Mang, J. Appl. Phys., 98 (2005) 064903.
- 4 J. Sun, M. L. Pantoya and S. L. Simon, Thermochim. Acta, (2006) in press.
- 5 W. Shufeng, Y. Hyunung, Y. Yangiang, and D. D. Dlott, Prop. Expl. Pyro., 30 (2005) 148.
- 6 A. Rai, S. Lee, K. Park and M. R. Zachariah, J. Phys. Chem. B, 108 (2004) 14793.
- 7 D. R. Lide, CRC Handbook of Chemistry and Physics, 79th Edition CRC Press Inc., 1998–1999.
- 8 Mallinckrodt Chemicals, J. T. Baker Molybdenum Trioxide MSDS, Mallinckrodt Baker, Inc. website retrieved Jan. 10, 2005.
- 9 H. J. Feng, J. J. Moore and D. G. Wirth, Proc. of the Symp. on Developments in Ceramic and Metal Matrix Composites, TMS Annual Meeting, TMS, San Diego, CA 1998, p. 219.
- 10 J. J. Granier, K. B. Plantier, K. B. Pantoya and M. L. Pantoya, J. Mater. Sci., 39 (2004) 6421.
- 11 M. A. Trunov, S. Mirko, Z. Xiaoying and E. L. Dreizin, Comb. Flame, 140 (2005) 310.
- 12 S. H. Fischer and M. C. Grubelich, Proc. of the 24th Int. Pyrotechnics Seminar, 1998.
- 13 K. Shimizu, R. C. Furneaux, G. E. Thompson, G. C. Wood, A. Gotoh and K. Kobayashi, Oxid. Met., 35 (1991) 427.
- 14 E. Suvaci, G. Simkovich and G. L. Messing, J. Am. Ceram. Soc., 83 (2000) 299.
- 15 M. A. Trunov, M. Schoenitz and E. L. Dreizin, Int. Workshop on Comb. and Prop., Novel Energetic Materials and Applications, Lerici, La Spezia, Italy (Sept. 2003).

DOI: 10.1007/s10973-005-7342-z